Article

Influence of the Laser Deposited 316L Single Layers on Corrosion in Physiological Media

Unai Garate [1,2], Enara Mardaras [3], Rodolfo González [3], Jon Iñaki Arrizubieta [2], Garikoitz Artola [3,*] and Javier Aldazabal [4,5,*]

1 MESHIND, Aliendalde 5, 48200 Durango, Spain; unai.garate@meshind.com
2 Department of Mechanical Engineering, University of the Basque Country, Plaza Torres Quevedo 1, 48013 Bilbao, Spain; joninaki.arrizubieta@ehu.eus
3 AZTERLAN, Basque Research and Technology Alliance (BRTA), 48200 Durango, Spain; emardaras@azterlan.es (E.M.); rgonzalez@azterlan.es (R.G.)
4 Tecnun School of Engineering, University of Navarra, Manuel Lardizabal 13, 20018 San Sebastian, Spain
5 Biomedical Engineering Centre, University of Navarra, Campus Universitario, 31080 Pamplona, Spain
* Correspondence: gartola@azterlan.es (G.A.); jaldazabal@tecnun.es (J.A.)

Abstract: A multilayer laser-deposited lining of AISI 316L stainless steel makes a regular structural steel surface corrosion resistant in physiological media. Despite the application of single-layer stainless-steel linings being economically beneficial and allowing thinner surface modifications, dilution effects that modify the pitting resistance of the coating must be accounted for. In order to study the feasibility of employing single-layer coatings instead of multilayer coatings for corrosion protection in physiological media, a polarization testing back-to-back comparison was performed between laser-deposited AISI 316L monolayers on 42CrMo4 quenched and tempered steel and cold-rolled AISI 316L sheet in Dulbecco's Phosphate Buffer Solution at 36 °C. A higher dispersion in pitting resistance, ranging from 800 mV to 1200 mV, was found on the coated samples, whereas the cold-rolled material was more stable in the 1200 mV range. The resulting differences in corrosion rates and pitting potentials open the discussion on whether the chemical composition deviations on AISI 316L dilution layers are acceptable in terms of surface functionality in medical devices.

Keywords: laser metal deposition; additive manufacturing; stainless steel; biomaterials; polarization; physiological media; corrosion; single layer; dilution

1. Introduction

Cast and wrought AISI 316L stainless steel (SS) is a well-established biomaterial for medical devices and implants, as is shown both in introductory literature to biomaterials science [1] and recent reviews in the field of orthopedic surgery and prosthetics [2]. Nevertheless, research focused on improving the performance of biomaterials is recently moving toward manufacturing processes involving powdered raw materials [3] instead of cast and wrought alternatives, as is also happening in other fields, such as aerospace [4]. This trend also affects 316L SS, and two working lines can be distinguished, depending on whether the improvement is focused on the bulk or the surface of the device.

Bulk improvement takes advantage of the possibility of controlling the porosity of the material by means of powder metallurgy [5,6]. More preferably, powder is processed through additive manufacturing technologies such as selective laser melting (SLM) to achieve controlled geometry scaffolds with a higher porosity design freedom than with conventional powder metallurgy [7–9] and research on further improving their dimensional accuracy is still ongoing [10]. The results offer the opportunity to tune the stiffness of the resulting part together with improved osteointegration thanks to the scaffold geometry control. Surface modification techniques instead of additive manufacturing processes are appealing for devices that do not benefit from these features.

The surface improvement approaches employing 316L SS and metallic powder involve different technologies, such as cold spraying [11] and laser cladding (LC), both with AISI 316L as the base [12] or as the cladded metal [13]. Both techniques allow different alloys to be combined in the substrate and the surface, applying the desired alloy on top of a less expensive or less biocompatible material. LC involves a metallurgical bonding with the substrate due to local melting, whereas cold spray produces a weaker mechanical bonding, which makes the former more reliable in terms of coating adhesion. However, the metallurgical bonding in LC generates a dilution between the filler and base material. The volume of the clad affected by the locally melted substrate is known as the dilution layer.

In the case of LC, this implies coating at least two layers of clad metal to avoid the contact of the dilution layer with the biological working media of the device or implant. Since working with single LC layers can be advantageous production- and geometry-wise, dilution and mixing effects of LC with AISI 316L have been studied in other fields of technology [14,15]. Nevertheless, little attention has been paid to the effect of single-coating dilution in the corrosion of the resulting surfaces when subjected to physiological conditions. This work is focused on extending the knowledge in this subject by studying a specific configuration that involves 316L SS cladded in a single layer on top of a 42CrMo4 quenched and tempered steel plate. The resulting dilution layer was afterwards submitted to corrosion by potentiodynamic polarization tests in Dulbecco's Phosphate Buffer Saline at 36 °C.

As any unexplored manufacturing approach must equal or exceed the performance of the existing alternatives, the results were assessed in light of the works mentioned above, some of which also shared potentiodynamic polarization results under several conditions [8,11–13], and a selected set of works the corrosion response of 316L SS in biological media [16–18]. The results point to a promising field of work that can yield proper performance but showed excessive variability in the studied setup.

2. Materials and Methods

2.1. Specimen Manufacturing

Two materials were chosen for the experimental work: the single-layer coated LC specimens, which are the object of study, and a reference wrought material, which was chosen to be a cold-rolled (CR) 316L SS of a thickness of 1 mm. The LC specimens were manufactured employing a Trumpf 3000 compact LC machine with a 316L SS powder grade on a 42CrMo4 quenched and tempered 25 mm-thick steel plate; see Figure 1a for the experimental setup. The chemical composition of the materials involved in the study is shown in Table 1. Helium gas was used for the powder particle carrier (4 L/min) and argon as a protective gas (12 L/min). The process parameters for AISI 316 SS were 1200 W laser power, 2 mm circular spot, 600 mm/min feed rate, and 6.5 g/min mass flow. These parameters were optimized in previous works carried out by the authors, and the deposited clad for the corrosion analysis is shown in Figure 1b. The employed LC layer thickness was 0.8 ± 0.1 mm with a dilution below 0.3 mm. The dilution resulted in a variation of the chemical composition of the AISI 316 SS powder, and real composition of the LC specimens is detailed in the last row of Table 1.

Table 1. Chemical composition of the materials that were employed the experimental work.

Material	C	Mn	Si	S	P	Cr	Ni	Mo
CR 316L SS	0.010	1.22	0.13	<0.005	<0.015	17.1	11.8	2.51
316L SS powder	0.011	1.49	2.30	<0.005	<0.015	17.0	12.0	2.95
42CrMo4 plate	0.42	0.75	0.20	<0.005	<0.015	1.10	-	0.22
LC specimens	0.041	1.28	2.10	<0.005	<0.015	15.1	10.8	2.63

(a)   **(b)**

Figure 1. (**a**) Experimental setup for sample manufacturing and (**b**) the deposited clad for the corrosion analysis.

It is worth noting that the 316L SS powder showed a significant deviation in the Si content from the reference CR 316L SS. This was due to the use of the Si as a protection for Cr depletion due to oxidation during the LC operation. This extra Si alloying is not used in wrought material, as the steel mills can use ladle metallurgy instead.

Attending to the chemical composition of the resulting LC specimen surfaces, it must be underlined that the dilution caused the Cr content to drop below the standard chemical composition limits of the 316L SS, whereas the C content was over the standard limits. Provided there is no Ti or Nb to fix the C, this could promote Cr carbide formation if cooling rates during LC were low enough.

In terms of microscopical characterization of the raw 316L SS powder, Figure 2 shows that under the scanning electron microscope (FEG-SEM ZEISS Ultra Plus, CARL ZEISS AG, Oberkochen, Germany) particles were very spherical and particle size ranged between 40 and 120 microns.

Figure 3 shows the SEM micrographs corresponding to specimen materials: the CR steel sheet (a) and the LC coating (b). It can be clearly seen that the cold-rolled reference sample (Figure 2a) was composed of a set of equiaxed recrystallized grains. This structure was generated by the recrystallization annealing that was applied after cold rolling to remove the strain hardening produced by the cold-rolling operation.

The sample under study (Figure 2b) showed a strong directionality due to solidification thermal gradients. This structure is a common outcome from welding processes: The base material works as a heat sink and produces a columnar growth of dendrites. As the cooling rate is higher than in arc welding, the dendrites are much finer than in usual welds. Furthermore, the LC sample showed signs of grain boundary segregation. The light grey phases had a higher atomic weight and thus reflected a brighter signal for the InLens detector of the SEM. This is attributable to a higher concentration of Cr and Mo in these areas, promoting the formation of ferrite and the corresponding depletion of the dark grey austenite grains. This observation was cross-checked by X-ray diffraction, confirming the presence of a cubic crystal system from space group lm3m in LC samples, which was identified as a ferritic stainless-steel structure with reference code 00-034-0396. The fact that the wrought reference steel was fully austenitic, and the LC specimens showed residual ferrite content, must be accounted for. This is an added difficulty to the already reduced Cr in the dilution layer when it comes to working in corrosive environments.
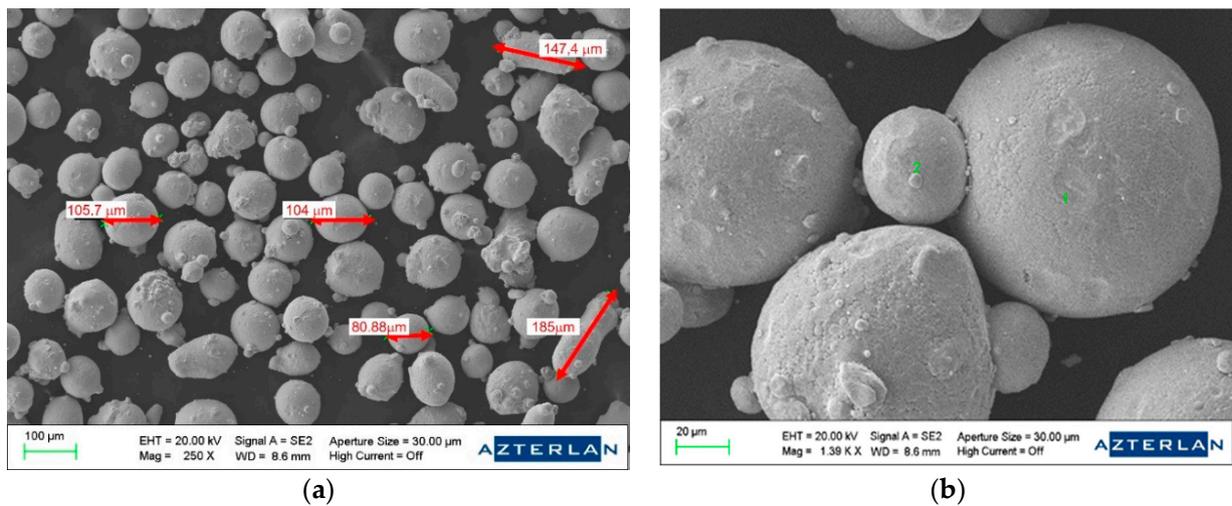
Figure 2. Scanning electron micrograph of the 316L SS powder employed in the manufacture of the specimens. Low magnification (**a**) and detailed close-up (**b**).
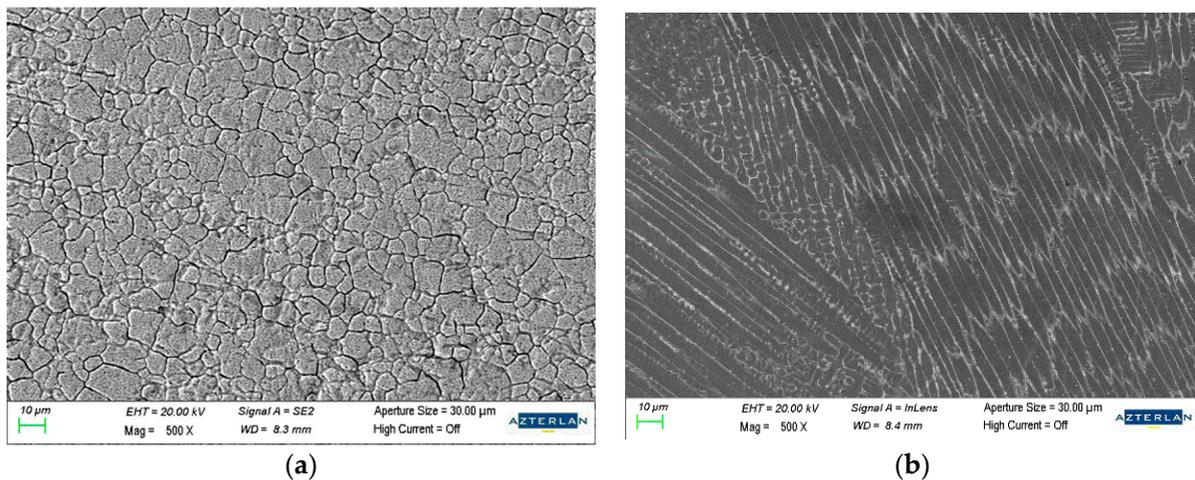

Figure 3. (**a**) As polished microstructure of the reference CR 316L SS. (**b**) As polished microstructure of the single-layer diluted LC specimens.

2.2. Corrosion Testing

The electrochemical tests were performed in an Autolab PGSTAT 302 N potentiostat/galvanostat (Metrohm AG, Herisau, Switzerland) with a three-electrode setup. The reference electrode (RE) was a saturated Ag/AgCl electrode, the counter electrode (CE) was made of platinum, and the LC specimens were connected as working electrodes (WE). The setup is shown in Figure 4: a standard double-wall cell (volume 0.30 L) with vertical fixing of the sample surface. The area of the WE exposed to the solution was 1 cm^2. Corrosion tests were performed in Dulbecco's Phosphate Buffer Solution (DPBS) (Lonza, Wlakersville, MD, USA) at 36 °C with the following chemical composition: 8.0% NaCl, 0.2% KCl, 1.15% Na$_2$HPO$_4 \cdot$2H$_2$O, and 0.2% KH$_2$PO$_4$. The measured pH of the DPBS was 7.0.

The open circuit potential (E$_{OCP}$) and potentiodynamic anodic polarization measurement tests were performed. All the tests were carried out at 36.5 ± 0.5 °C. The corrosion potential E$_{CORR}$ was determined from E$_{OCP}$ vs. time curves when the stable or quasi-steady-state potential was reached. The variation in E$_{OCP}$ was recorded for 1.5 h. The potentiodynamic anodic polarization involved sweeping potential from −0.2 V to 1.5 V at a scan rate of 0.166 mV/s with continuous measurement. All the electrochemical measurements were replicated at least three times to confirm the reproducibility of the tests. Corrosion curves were obtained both for the LC specimens and the cold-rolled 316L SS

specimens for comparison purposes. All specimen surfaces were mechanically mirror polished by a sequence of SiC grinding in sandpaper and subsequent diamond suspension polishing to a roughness Ra < 0.2 µm prior to all tests.
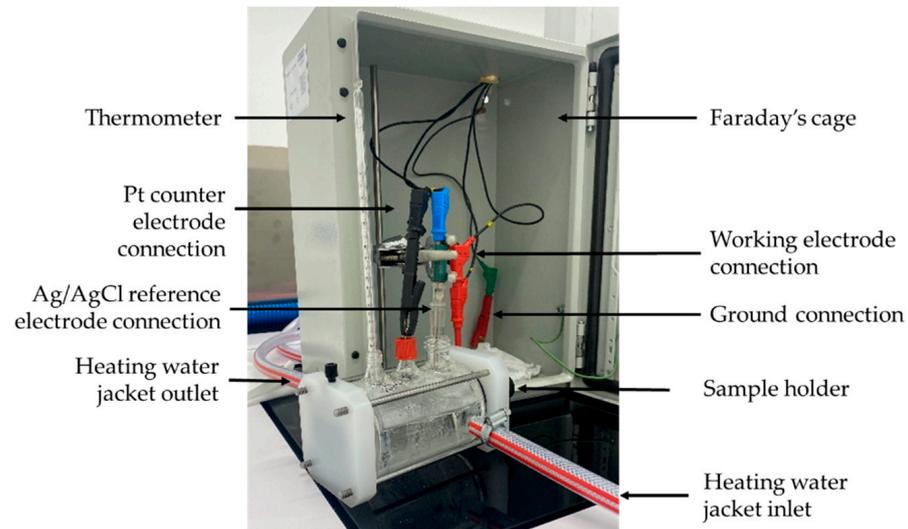

Figure 4. Corrosion cell setup employed for experiments.

3. Results

Figure 5 shows the three repeats of the OCP curves for both the reference wrought CR 316L SS, namely, PH1, PH2, and PH4 (a), and for the single-layer LC specimens of interest, namely, LH1, LH2, and LH3 (b). Similar OCP values were observed for both materials, including the dispersion of the results to the sides within a 0.20 mV distance. It is noticeable that for the reference steel, the fact of having dispersion did not induce serrated curves, whereas the LH1 sample from the diluted LC 316L SS samples performed erratically.
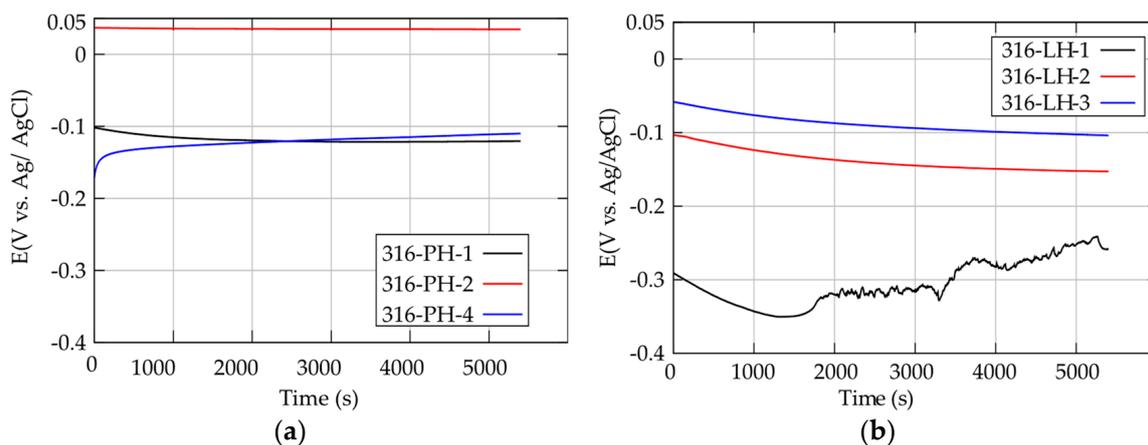

Figure 5. Variation in time of the open-circuit potential (E_{OCP}) for CR 316L SS (**a**) and LC single-layer dilution 316L SS (**b**) in PBS solution at 36 °C.

Figure 6 shows the repeat set of polarization curves for both reference and study materials. It is noteworthy that the position of the corrosion potential confirms the observation in the OCP tests, as both materials showed a Tafel area in the same range of voltages. Regarding passive layer breakdown voltages, both materials reached 1200 mV, with the reference material being the one with the more repeatable behavior in this parameter. The LC single-layer dilution 316L SS showed a trend towards lower breakdown voltages. Thus, despite the drawbacks of lower Cr content and the presence of ferrite, the diluted LC layer

can perform in DPBS occasionally as well as the more controlled, fully austenitic reference CR 316L SS, whose chemical composition fulfils the standards. LH1 early breakdown could be attributable to the incipient crevice observed in the surface but is kept for the record.
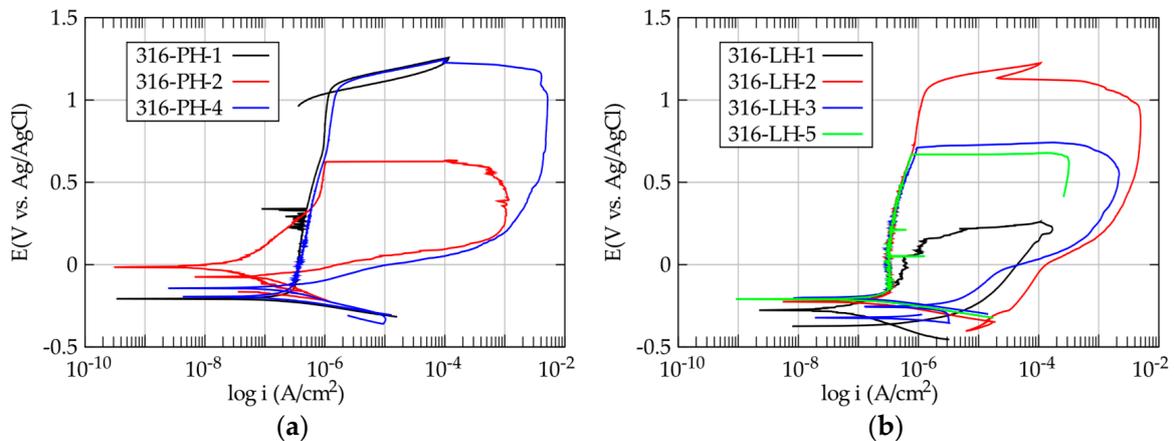

Figure 6. Potentiodynamic polarization curves for CR 316L SS (**a**) and LC single-layer dilution 316L SS (**b**) in PBS solution at 36 °C.

4. Discussion

Working with single-layer LC and 316L SS on low-alloy steels leads to a chemically and microstructurally unfavorable condition when compared to wrought materials. Nevertheless, and despite the Cr reduction and the presence of ferrite, it turns out that the diluted 316L SS can behave in DPBS as well as a standard fulfilling supply of wrought 316L. When breaking down the comparison to what would be the most similar and the most dissimilar behaviors, Figure 7a shows that at least in one of the tested surfaces the theoretical disadvantage of the diluted coating was meaningless for corrosion in DPBS at body temperature. This yielded a pitting resistance (PR) of 1200 mV, calculated as the passive layer breakdown potential (E_{BD}) minus the corrosion potential (E_{CORR}).
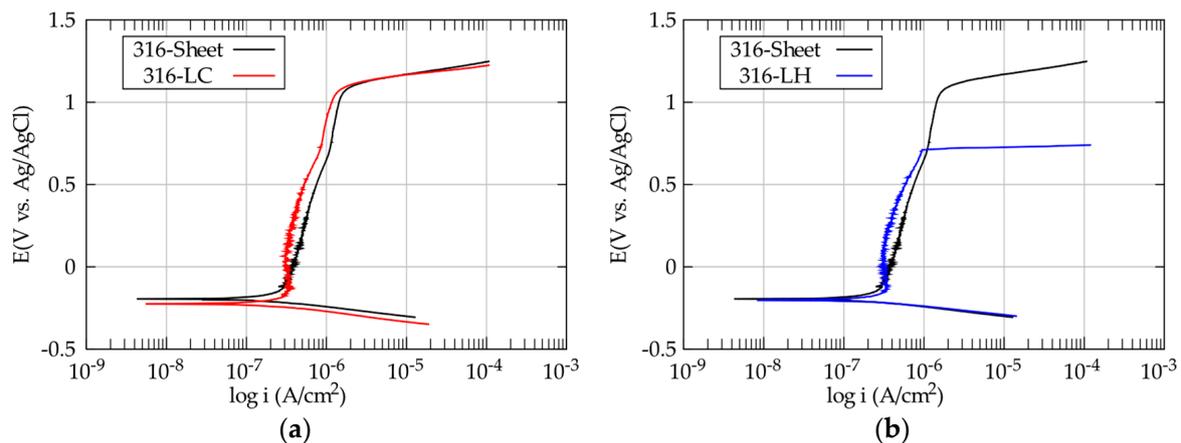

Figure 7. (**a**) Highest similarity and (**b**) highest dissimilarity found between the corrosion behaviors of CR 316L SS and LC single-layer dilution 316L SS in PBS solution at 36 °C.

This fits with the results from Lodhi et al. [8], whose polarization testing showed that additively manufactured (SLM) 316L SS can outperform the wrought alternative in terms of the PR. Their average PR values were in the range between 1100 and 1300 mV when testing the SLM processed material in usual media such as DPBS, human serum, or 0.9 M NaCl solution in distilled water. Actually, the results in DPBS were in the middle of the interval, close to 1200 mV. Human serum was the most aggressive media and 0.9 NaCl

the least. Lodhi et al. attributed a significant weight to the fast solidification of the SLM. Despite the power and heating involved with single-layer LC being higher than what is employed for SLM, the thickness of the substrate and the use of a thickness around 0.7 mm sets a good scenario to apply Lodhi's theory to the observations in Figure 7a.

The same tests [8] in wrought steel samples yielded PR values between 400 mV and 700 mV, which are closer to the PR of 800 mV observed in Figure 7b for the diluted sample. So, despite steel outperforming wrought steel in [8], this assertion cannot be transferred to the LC dilution case, except if only the best corrosion behavior in Figure 7a is taken and compared to the wrought steel in [8].

The results in [8] were especially relevant for comparison, as the media employed for the polarization was the same as that used in the dilution-layer exploration. When opening the frame to other biological or physiological media, further misfits arise. The work from Dikici et al. [11] performed the polarizations on Ringer's solution over cold-sprayed 316L, which was annealed at increasing temperatures. In this case, PR dropped from 500 mV to 300 mV after annealing the 316L layer over 750 °C. Provided the Cr-rich sigma phase appeared at these high temperatures, leading to a Cr depletion in the austenitic phase, an analogy can be drawn with the observations in the LC dilution zone microstructures. The LC showed heterogeneities that would fit with some more depleted areas in Cr and with higher segregation. Furthermore, the temperature of the substrate grew during the cladding process, which reduced the cooling rate, thus leading to a higher risk of sigma-phase appearance, higher segregation, and less of the high cooling rate effect observed in [8].

This rationale fits with the measurement of PR values close to 400 mV by Liu et al., as in [13] the manufacturing approach was multilayered LC. This strategy usually leads to overheating the specimen and reduced cooling rates. Thus, despite the chemical compositions in [13] matching the powder chemistry by avoiding dilution, overheating could be more important than Cr depletion and the presence of ferrite. This statement should be considered with care, as the testing media employed by Liu et al. was simulated body fluid that is more aggressive than PBS and could have hindered solution-related phenomena.

When recurring to other corrosion works on biomedical 316L polarization for cross-checking the observations above [16–18], the same orders of magnitude are found. Lafiti et al. [16] reported PR values over 1100 mV in wrought materials, confirming the results obtained with CR 316L SS samples in this work. Majumdar [17] came to the same conclusion as Lodhi [8] on the improvement in corrosion caused by the high cooling rates from laser melting. Finally, Hryniewicz and Roskosz [18] showed that surface finish differences in 316L in Ringer's solution could produce a change in PR from 700 mV to 1200 mV, confirming that surface heterogeneities can explain the dispersions observed in Figure 6b.

5. Conclusions

The assessment of the results in light of the existing literature allows the following conclusions to be drawn regarding the feasibility of employing single-layer LC coatings of 316L SS for biomedical applications:

- Despite the use of single layers causing a reduction in Cr content and its distribution in the diluted 316L SS LC coating, if the material is cooled down at a sufficient rate the benefit of undercooling apparently exceeds the drawbacks of segregation and dissolved Cr loss.
- The diluted single-layer LC 316L SS coating can perform locally as well as a wrought counterpart.
- All in all, the results are way too disperse, and having a very promising performance locally does not allow the wrought counterpart to be substituted by an LC-coated alternative. The specific conditions employed in this work are not applicable in biomedicine. Just one spot of corrosion becomes the weak chain in the link and would ruin the entire medical device.

Thus, in summary, employing LC single layers as biomaterials is only feasible if process conditions are repeatable across the whole coated surface; furthermore, these conditions must ensure high cooling rates, similar to those achieved in SLM.

Conflicts of Interest: The authors declare no conflict of interest.

References

1. Ratner, B.D.; Hoffman, A.S.; Schoen, F.J.; Lemons, J.E. *Biomaterials Science: An Introduction to Materials in Medicine*, 2nd ed.; Elsevier Academic Press: San Diego, CA, USA, 2004; pp. 141–143.
2. Szczęsny, G.; Kopec, M.; Politis, D.J.; Kowalewski, Z.L.; Łazarski, A.; Szolc, T. A Review on Biomaterials for Orthopaedic Surgery and Traumatology: From Past to Present. *Materials* **2022**, *15*, 3622. [CrossRef] [PubMed]
3. Ibrahim, M.Z.; Sarhan, A.A.D.; Yusuf, F.; Hamdi, M. Biomedical materials and techniques to improve the tribological, mechanical and biomedical properties of orthopedic implants—A review article. *J. Alloys Compd.* **2017**, *714*, 636–667. [CrossRef]
4. Khorasani, M.; Ghasemi, A.H.; Rolfe, B.; Gibson, I. Additive manufacturing a powerful tool for the aerospace industry. *Rap. Prot. J.* **2022**, *28*, 87–100. [CrossRef]
5. Dewidar, M.M.; Khalil, K.A.; Lim, J.K. Processing and mechanical properties of porous 316L stainless steel for biomedical applications. *Trans. Nonferrous Met. Soc. China* **2007**, *17*, 468–473. [CrossRef]
6. Noor, F.; Jamaludin, K.R.K.; Ahmad, S. Fabrication of Porous Stainless Steel 316L for Biomedical Applications. *MATEC Web Conf.* **2017**, *135*, 00062. [CrossRef]
7. Capek, J.; Machová, M.; Fousová, M.; Kubásek, J.; Vojtech, D.; Fojt, J.; Jablonska, E.; Lipov, J.; Rumi, T. Highly porous, low elastic modulus 316L stainless steel scaffold prepared by selective laser melting. *Mat. Sci. Eng. C* **2016**, *69*, 631–639. [CrossRef] [PubMed]
8. Lodhi, M.J.K.; Deen, K.M.; Greenlee-Wacker, M.C.; Haider, W. Additively manufactures 316L stainless steel with improved corrosion resistance and biological response for medical applications. *Add. Manuf.* **2019**, *27*, 8–19. [CrossRef]
9. Cosma, C.; Kessler, J.; Gebhardt, A.; Campbell, I.; Balc, N. Improving the Mechanical Strength of Dental Applications and Lattice Structures SLM Processed. *Materials* **2020**, *13*, 905. [CrossRef] [PubMed]
10. Giganto, S.; Martinez-Pellitero, S.; Cuesta, E.; Zapico, P. Proposal of design rules for improving the accuracy of selective laser melting (SLM) manufacturing using benchmark parts. *Rap. Prot. J.* **2022**, *28*, 1129–1143. [CrossRef]
11. Dikici, B.; Topuz, M. Production of Annealed Cold-Sprayed 316L Stainless Steel Coatings for Biomedical Applications and Their in-vitro Corrosion Response. *Prot. Met. Phys. Chem. Surf.* **2018**, *54*, 333–339. [CrossRef]
12. Kumar, A.; Roy, S.K.; Berger, H.; Majumdar, J.D. Laser Surface cladding of Ti-6Al-4V on AISI 316L Stainless Steel for Bio-Implant application. *Lasers Eng.* **2014**, *28*, 11–33.
13. Liu, Y.; Yang, J.; Yang, H.; Li, K.; Qiu, Y.; Zhang, W.; Zhou, S. Cu-bearing 316L stainless steel coatings produced by laser melting deposition: Microstructure and corrosion behavior in simulated body fluids. *Surf. Coat. Tech.* **2021**, *428*, 127868. [CrossRef]
14. Bloemer, P.R.A.; Pacheco, J.T.; Cunha, A.; Veiga, M.T.; de Moura Filho, O.C.; Meura, V.H.; Teixeira, M.F. Laser Cladding of Inconel 625 on AISI 316L: Microstructural and Mechanical Evaluation of Parameters Estimated by Empirical-Statistical Model. *JMEPEG* **2022**, *31*, 211–220. [CrossRef]
15. Muro, M.; Leunda, J.; Artola, G.; Soriano, C. Microstructural Tuning of a Laser-Cladding Layer by Means of a Mix of Commercial Inconel 625 and AISI H13 Powders. *Materials* **2019**, *12*, 544. [CrossRef] [PubMed]
16. Latifi, A.; Imani, M.; Khorasani, M.T.; Joupari, M.D. Electrochemical and chemical methods for improving surface characteristics of 316L stainless steel for biomedical applications. *Suf. Coat. Tech.* **2013**, *221*, 1–12. [CrossRef]
17. Majumdar, J.D.; Kumar, A.; Pityana, S.; Manna, I. Laser Surface Melting of AISI 316L Stainless Steel for Bio-implant Application. *Proc. Natl. Acad. Sci. India Sect. A Phys. Sci.* **2018**, *88*, 387–403. [CrossRef]
18. Hryniewicz, T.; Rokosz, K. Corrosion resistance of magnetoelectropolished AISI 316L SS biomaterial. *Anti-Corr. Meth. Mats.* **2014**, *61*, 57–64. [CrossRef]